PIER C

(Received 17 September 2025, Accepted 24 November 2025, Scheduled 8 January 2026)

Numerical and Experimental Analysis of a Reversible Damage Model for Millimeter-Wave Diagnostics of Glass Fiber Reinforced Polymer Structures

Manuel E. Rao[1,*], Jochen Moll[1], Maximilian Ebel[2], Peter Kraemer[1], and Viktor Krozer[2]

[1] *Department of Mechanical Engineering, University of Siegen, Paul-Bonatz-Straße 9-11, Siegen 57076, Germany*
[2] *Department of Physics, Goethe University Frankfurt, Max-von-Laue-Straße 1, Frankfurt 60438, Germany*

ABSTRACT: In this work, a delamination model for millimeter-wave inspections of glass fiber reinforced polymer (GFRP) is proposed that replicates the scattering characteristics of a real delamination. The model can be used not only for the performance assessment of conventional nondestructive testing (NDT) approaches, but also for structural health monitoring (SHM) applications with permanently installed radar sensors in the frequency band from 57 to 65 GHz. Parametric numerical and experimental investigations were carried out for three different cases: (a) delamination represented by two GFRP plates with a defined air gap between the plates, (b) erosion protection tape above a GFRP plate separated by an air gap, and (c) erosion protection tape on top of a rigid foam that has similar dielectric properties to air. All signals have been processed using a damage indicator approach (DI). The numerical and experimental results show a high degree of similarity in the DI curve as a function of the delamination thickness. The differences between simulation and experiment are between 0 and 0.3 mm in delamination thickness. Hence, the proposed model can be used for the qualification of radar-based NDT and SHM systems for various practical applications, e.g., wind turbine blades (WTBs), eliminating the need for expensive, destructive testing.

1. INTRODUCTION

The need for nondestructive testing (NDT) methods, which must be customized for individual applications, has rapidly increased. Specifically, structural health monitoring (SHM) with permanently installed sensors contributes to the improvement of structural integrity and reliability of material systems. Damage should be detected at an early stage using suitable sensors and algorithms [1]. In recent years, composite materials have been widely used in the design of technical structures due to their low density, high corrosion resistance, and mechanical stiffness [2]. This shows the need that SHM methods must be applicable to composite structures as well, e.g., to detect delaminations.

Electromagnetic (EM) waves in the frequency range from 300 MHz to 300 GHz have proven to be suitable for NDT inspections [3]. In this context, frequency modulated continuous wave (FMCW) radars are widely used to resolve targets in distance domain [4]. An example is given by the successful damage detection during a full-scale fatigue test of a 31 m long wind turbine blade (WTB) using 40 FMCW radars at 60 GHz [5]. In addition, an embedded FMCW radar application in a multilayer aerospace composite laminate can be found in [6]. The FMCW radar can also detect vibration displacements using the example of a fiberglass sandwich panel [7], a bridge model in the laboratory [8], or a pedestrian bridge [9].

Varying environmental and operational conditions pose a challenge in signal processing and interpretation for automated damage assessment. Changes over time in external parameters such as temperature, humidity, wind, mass loading, and vibrations influence the measured signals [10]. Mahendran et al. [11] performed measurements with an FMCW radar to demonstrate phase shifts in the signal with different temperature and humidity settings. Simon et al. [12] compensated for the trend of the temperature in the radar signals, which were measured during a full-scale fatigue test of a WTB with FMCW radars. Machine learning techniques are used in [13] to extract features from extensive data sets with various real-world scenarios. In the context of WTB monitoring, Streser et al. [14] trained and tested a conventional convolutional neural network with data obtained during a full-scale fatigue test [5].

Delaminations are a type of damage in composite structures that are characterized by the detachment of adjacent fiber layers. This type of damage can be modeled as a three-layer system, where the middle layer is represented by air. Based on this understanding, He et al. [15] investigated a delamination in a thin asphalt pavement using ground penetrating radar (GPR). A GPR was also used in the work of Liu et al. [16] for the monitoring of reinforced concrete pavements. Near-surface delaminations and voids on a concrete test slab were detected by Popovics et al. [17] using a synthetic aperture radar combined with acoustic impact-echo imaging.

It is important for delamination modeling to consider delamination growth and relevant delamination dimensions [18].

* Corresponding author: Manuel E. Rao (manuel.rao@uni-siegen.de).

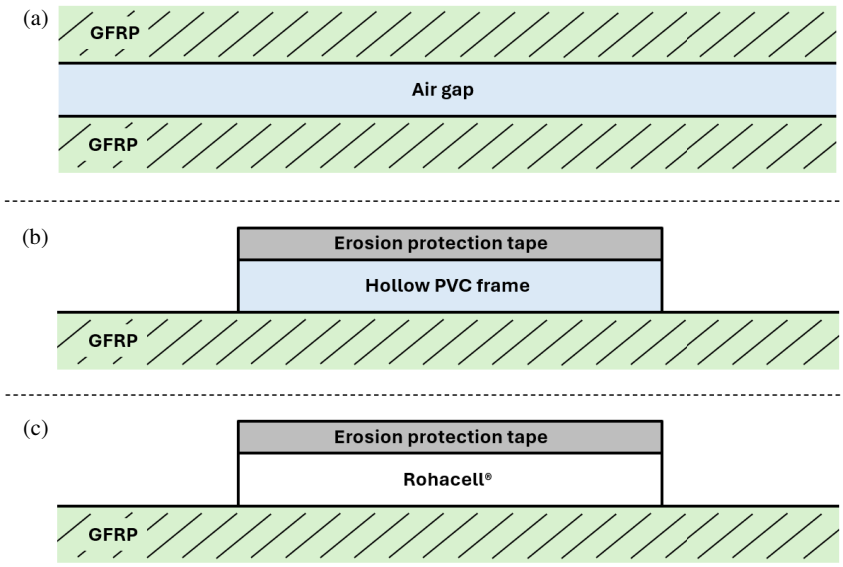

FIGURE 1. Schematic representation of the three-layer delamination model for the cases: (a) delamination, (b) reference damage model with erosion protection tape (reference damage model #1), and (c) air gap replaced by a layer of Rohacell® (reference damage model #2).

Eun et al. [19] modeled a multi-layer Dallenbach radar absorber with glass/epoxy and glass/epoxy-multiwall carbon nanotubes with delamination thicknesses from 0.1 mm to 0.5 mm. Xu et al. [20] inspected a 16-layer CFRP structure using the eddy current method with T-R pancake coil, in which a 20 mm × 20 mm teflon film with a thickness of 0.125 mm was inserted between different layers as a representative delamination. Akbar et al. [21] performed time domain reflectometry on a 152 mm × 110 mm GFRP sample with 20 different delaminations from 10 mm × 10 mm × 1 mm to 20 mm × 20 mm × 15 mm.

The novelty of this work lies in the design, realization, and characterization of a reversible reference damage model for the imitation of a delamination in GFRP without compromising the structure itself. Here, the reference structure is defined as the intact structure, which severs as the baseline for comparison with damaged structures in SHM algorithms. The damage model has a sandwich design consisting of three layers, which is investigated numerically and experimentally from 57 GHz to 65 GHz. Figure 1 shows the overall concept for three different cases:

(a) Delamination: Two GFRP plates are separated from each other with an increasing air gap using steps of 0.1 mm.

(b) Reference damage model #1: Erosion protection tape is stretched over a hollow PVC frame to replace the upper GFRP plate. Similar to before, the erosion protection tape can be translated in steps of 0.1 mm to change delamination thickness.

(c) Reference damage model #2: To increase mechanical stability, the erosion protection tape is attached to a layer of Rohacell® with a specific thickness to replace the air gap by solid rigid foam.

Only one material change was made in each step to identify the smallest deviations for the conception of the final damage model (c).

A reversible damage model, as proposed here, has a large impact on the effective experimental qualification of SHM systems, which requires comprehensive destructive experiments for the probability of detection (POD) assessment. These tests are time-consuming and extremely costly. In the context of ultrasonic SHM, Moll et al. [22] successfully used a reversible damage model attached to the surface of a carbon fiber composite plate to model the scattering characteristics of a delamination.

The remainder of this paper is structured as follows. The subsequent Section 2 describes the numerical modeling in the target frequency range using Computer Simulation Technology (CST) Microwave Studio. In Section 3, all three approaches shown in Figure 1 are experimentally set up and measured in the laboratory. The numerical and experimental results are presented in Section 4 using a damage indicator (DI) approach. Section 5 contains a summary and a brief outlook of future research.

2. NUMERICAL MODELING

2.1. Simulation Model and Dielectric Material Properties

The numerical modelling starts with the case of the delamination, where the distance between two GFRP plates with scaled geometric dimensions of 25 mm × 25 mm × 0.5 mm is filled with air. The air gap between the plates can vary in steps of 0.1 mm to model delaminations of different thicknesses, see Figure 2. The distance between the signal source, denoted as waveguide port, and the first interface, which is the front GFRP plate, is defined by L. Four distances are investigated in the simulation: 12.5 mm, 25 mm, 37.5 mm and 50 mm. The size of the delamination, i.e., the distance between the GFRP plates, is given by d and ranges from 0 mm to 13 mm. The GFRP plates can be moved away from or towards the signal source.

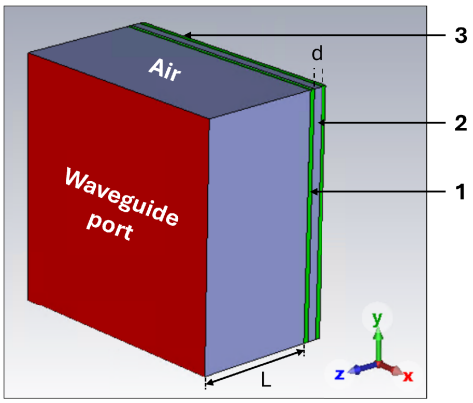

FIGURE 2. Simulation model of a three-layer system in CST Microwave Studio. L denotes the distance from the radar to the first interface and d the thickness of the delamination and reference damage, respectively. The numbers are explained in Table 1.

Next, the design of the reference damage model #1 replaces the upper GFRP plate by erosion protection tape specifically designed for the application in WTBs. The tape is based on polyurethane (PU) as carrier material with a thickness of 0.3 mm and an adhesive layer with a thickness of 0.06 mm. Finally, reference damage model #2 replaces the air gap by Rohacell® material which is specifically designed for high-frequency applications and has similar dielectric properties to air. The solid foam is light-weight, improves the mechanical stability, and keeps the delamination thickness constant.

The three models of the three-layer system were modeled in CST Microwave Studio. EM simulations were carried out with open boundaries and the time domain solver in the frequency range from 57 GHz to 65 GHz, as this frequency range is also provided by the FMCW radar used for the experimental studies. In CST, a Gaussian pulse is used to excite plane EM waves at the defined waveguide port at the rectangular cross section. The reflected pulses are detected again at the waveguide port. The material systems are described in Table 1 with the material properties listed in Table 2.

A graphics processing unit (GPU) was used for the simulations. It consists of an AMD Ryzen 3950X processor with 16 cores, a 128 GB random-access memory (RAM) and a 32 GB Nvidia Quadro GV100 graphics card. In this high-frequency range, the grid cells in the simulation are very fine, which is why the defined dimensions are scaled 20 times smaller compared to the experimental setup due to limited RAM. The delamination thickness d and the thickness of the erosion protection tape were modeled in the correct dimensions.

TABLE 1. Materials of the three-layer system: delamination, reference damage model #1 and reference damage model #2.

Dam. model \ Material no.	1	2	3
Delamination	GFRP	Air	GFRP
Ref. dam. #1	GFRP	Air	PU
Ref. dam. #2	GFRP	Rohacell®	PU

TABLE 2. Dielectric properties of the three layer system, where ε_r' is the real part of the permittivity, $\tan(\delta)$ the dielectric loss tangent and f the frequency.

Material	ε_r'	$\tan(\delta)$	f (GHz)	Reference
Air	1.00059	0	n. s.	CST
GFRP	5.5	0.04	1 MHz	Data sheet
PU	3.5	0.1	10 GHz	[23]
Rohacell®	≈ 1.1	≈ 0.01	2.5–26.5 GHz	Data sheet

2.2. Physical Interpretation of Simulated Signals

Figure 3 shows the simulated signals in the time domain for the case of delamination in terms of typical delamination thicknesses $d = 0.1$ mm, 0.2 mm, 0.5 mm, 1 mm, and 2.5 mm. The radar distances $L = 12.5$ mm and 50 mm were selected here exemplarily for the output signals. The delamination thickness was increased away from the radar. The input signals are the same for all L and d.

Compared to the input signals, the output signals are shifted in time after

$$\Delta t = \frac{2L\sqrt{\varepsilon_r'\sqrt{1+\tan^2(\delta)}}}{c_0}, \tag{1}$$

where c_0 is the speed of light, ε_r' the real part of the permittivity, and $\tan(\delta)$ the dielectric loss tangent for non-magnetic materials [24, 25]. The factor 2 results from the double distance length with a reflection at an interface.

The first echo is assumed as the main contribution to the output signal in Equation (1), because all other echoes already have less signal energy due to previous reflections. For $L = 50$ mm, two more peaks can be seen, each occurring after a further 100 mm. In addition, the reference state ($d = 0$ mm) has two fewer boundary conditions than the damaged state ($d > 0$ mm). Hence, the total reflectivity increases with the number of interfaces, as there is another share in reflection at each interface. The highest reflectivity is given for $d = 1$ mm.

A frequency domain representation is shown in Figure 4. The increase of the intensity is confirmed from $d = 0$ mm to 1 mm. The similarity of the trends for $d = 0.5$ mm and 1 mm as well as a decrease of the signal intensity until 2.5 mm is recognizable. More minima (dips) can be seen in the signals for $L = 50$ mm, indicating a higher correlation of the radar distance with the transmission behavior. More oscillations of the EM waves appear for larger L.

Taking into account the inverse of Equation (1), considering basically the first echo again, the dips are discretized in this one-dimensional problem in frequencies

$$f_m = \frac{c_0}{2L\sqrt{\varepsilon_r'\sqrt{1+\tan^2(\delta)}}}\, m \tag{2}$$

where m is the number of the wave mode [25]. At frequency intervals $f_m - f_{m-1}$, oscillations are possible as multiples of half the wavelength λ within L. The dips occur for $L = 50$ mm every 3.00 GHz, as can be verified in Figure 4(b).

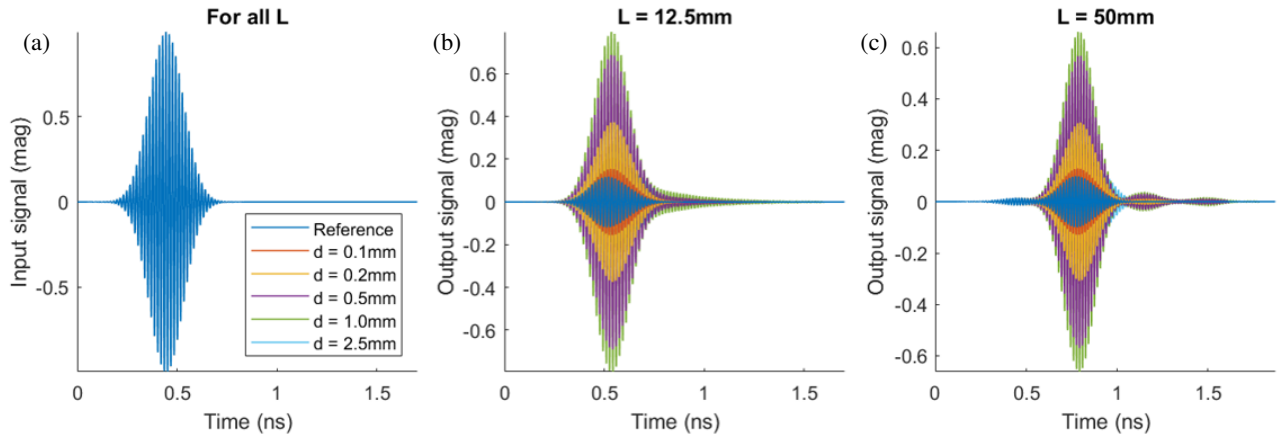

FIGURE 3. Simulated signals in the time domain for typical delamination thicknesses d directed away from the radar. The radar distances are (b) $L = 12.5$ mm and (c) 50 mm to demonstrate exemplary the increasing time difference between (a) the input signal and (b)–(c) the corresponding output signal by increasing L.

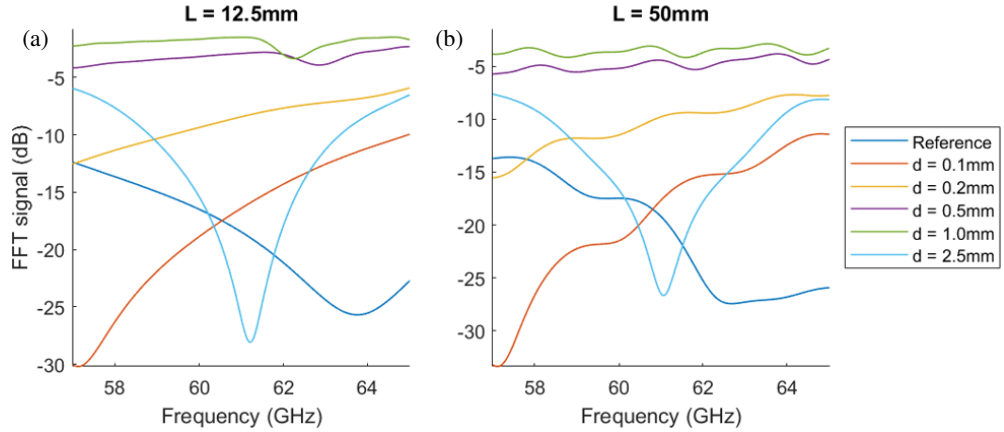

FIGURE 4. Simulated signals in the frequency domain for typical delamination thicknesses d directed away from the radar. The radar distances are (a) $L = 12.5$ mm and (b) 50 mm to demonstrate exemplary the frequency dependence of the reflection intensity. The highest intensity is given at $d = 1$ mm. The greater the radar distance L, the more frequencies influence the transmission behavior of EM waves through the interface.

$\lambda/2$ can be calculated by converting Equation (2) to $L = \lambda/2$ and setting $m = 1$. This results in 2.50 mm for 60 GHz. L was chosen accordingly as a multiple of 2.50 mm for the numerical model and the experimental setup. Theoretically expected, the signal intensities have a periodic extremum every $d = \lambda/2$. Damage detection in the time domain will therefore essentially depend on the signal intensities.

3. EXPERIMENTAL SETUP

3.1. Description of Reference Damage Realization

Figure 5 shows a drawing of the experimental setup and Figure 6 its practical realization. In the case of the delamination experiment, see Figure 1(a), two rectangular GFRP plates from CG TEC GmbH with the dimensions of 500 mm × 500 mm × 10 mm have been used. Only the lower GFRP plate is fixed to the vertical aluminum profiles. The upper GFRP plate can be moved upwards using micrometer screw gauges of type 148-104-10 from Mitutoyo with a nonius scale accuracy of 0.01 mm.

Measurements were performed from 0 mm to 11 mm in steps of 0.1 mm. The three-layer system can be moved vertically to change the distance to the radar L. Four lengths were chosen for the measurements series: 250 mm, 500 mm, 750 mm and 1000 mm. The radar is centrally positioned below the GFRP plate to measure the increase in the delamination thickness d directed away from the radar (radar position 1). In another experiment, the radar is screwed to a wooden plate to study variable damage size towards the radar (radar position 2).

Figure 6(b) shows the realization of reference damage #1, see Figure 1(b). A transparent erosion protection tape of type *Wind Protection Tape 2.0* from 3M™ was stretched over a PVC frame. At the beginning of the measurement series, the PVC frame is placed on top of the GFRP plate with the erosion protection tape in direct contact with the GFRP plate. Micrometer screw gauges are used at the corners of the PVC frame to increase delamination thickness in steps of 0.1 mm.

The frame has the dimensions of 250 mm × 250 mm × 15 mm, which means that the reference damage #1 does not cover the entire GFRP plate. However, assuming an azimuthal radiation of the dielectric lens antenna of 8° at a distance of $L = 1000$ mm leads to an inspection area on the specimen with a diameter of 140 mm which is significantly smaller than the di-

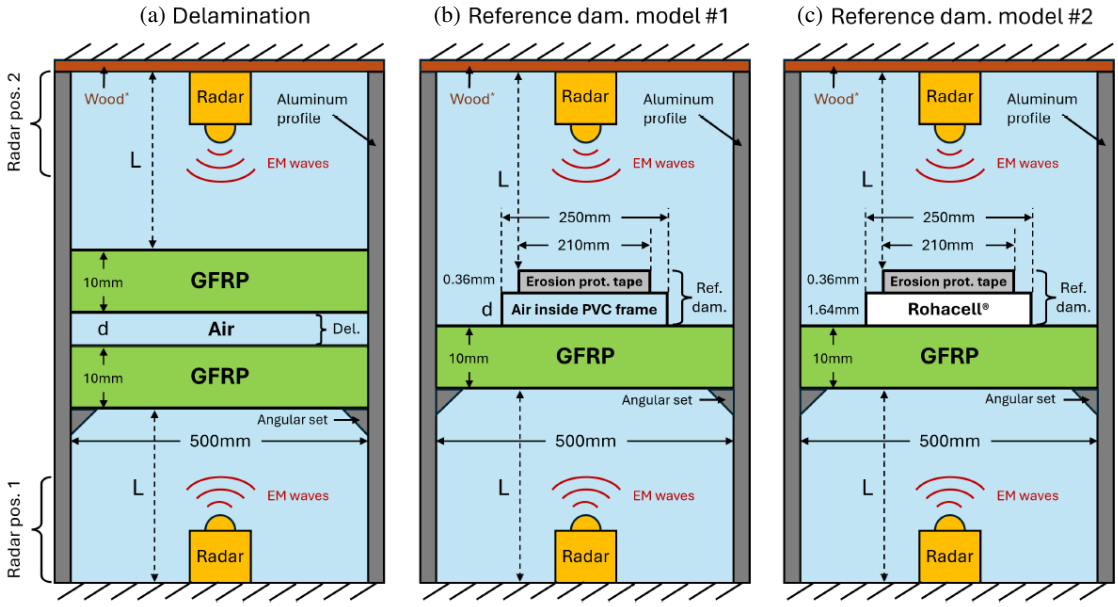

FIGURE 5. Illustration of the three-layer systems in the laboratory: (a) delamination, (b) reference damage model #1, and (c) reference damage model #2. The wooden plate with mounted radar is only necessary for radar measurements, when the damage size is changed towards the radar (radar position 2). For the damage directed away from radar, the radar is placed on an optical table (radar position 1). Aluminum profiles and angular sets are used to improve the stability of each setup. L denotes the distance from the radar to the first interface and d the thickness of the delamination.

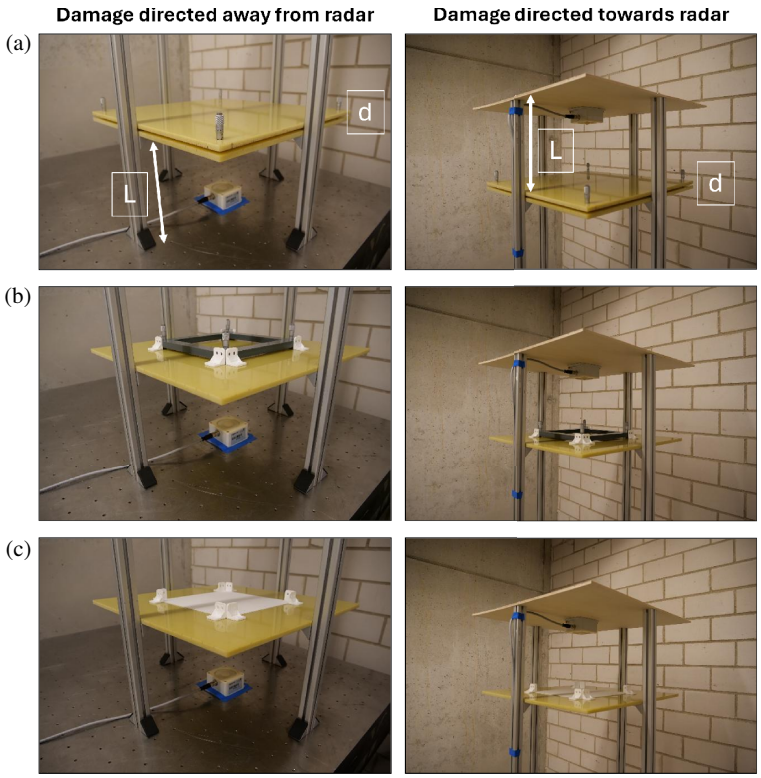

FIGURE 6. Experimental setup showing (a) delamination, (b) reference damage model #1, and (c) reference damage model #2. On the left side, the delamination thickness increases away from the radar, and on the right side towards the radar. L denotes the distance from the radar to the first interface and d the delamination thickness.

mension of the frame. Because of this, the measurements solely include the effect of the EM waves with the reference damage #1.

Figure 6(c) shows the final experimental setup with reference damage #2, see Figure 1(c). The transparent erosion protection tape is now attached to a Rohacell® sheet to enhance mechanical stability. Rohacell® 51 HF from Gaugler & Lutz was ex-

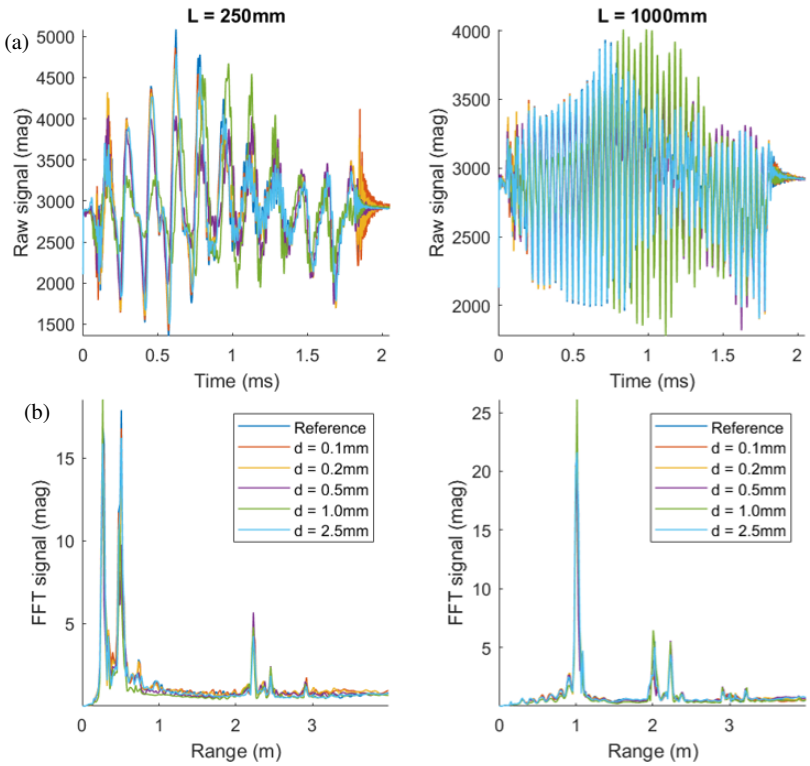

FIGURE 7. (a) Experimental measurements for typical delamination thicknesses d directed away from the radar. The radar distances are $L = 250$ mm (left) and 1000 mm (right). (b) FFT-processed radar signals.

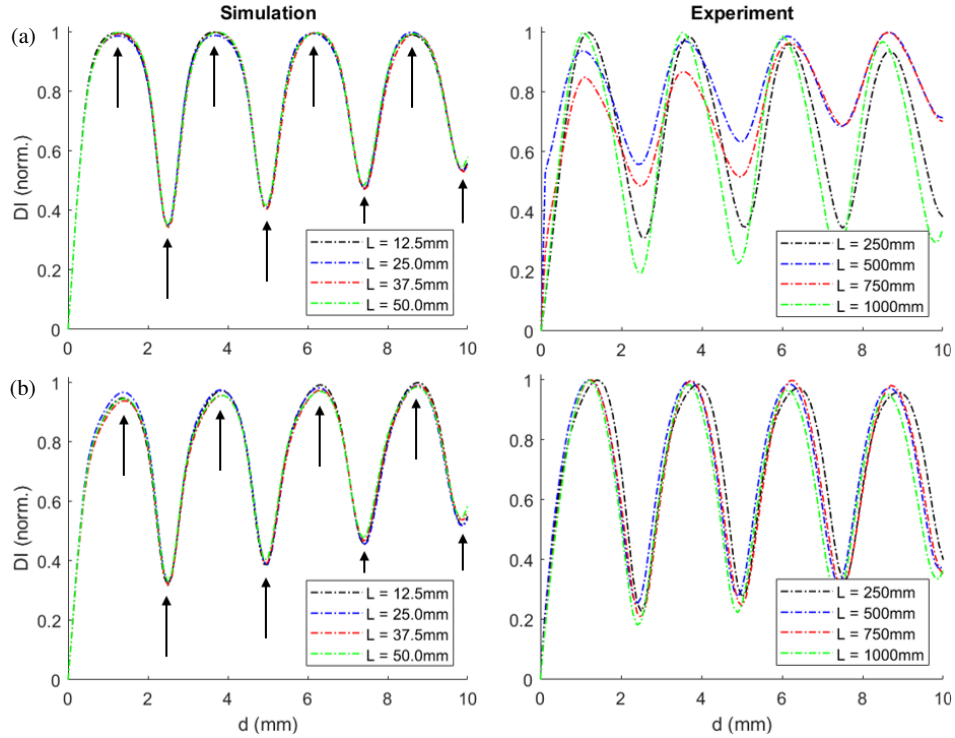

FIGURE 8. DI as a function of delamination thickness d directed (a) away from the radar and (b) towards the radar in four different radar distances L. The damage size step width is 0.1 mm. The black arrows on the left indicate the extrema.

plicitly selected, because it is a lightweight solid foam, has similar dielectric properties to air and can be manufactured with a minimum thickness of 1 mm. As shown later in the DI trends depicted in Figure 8 and Figure 9, a thickness of 1.25 mm would be optimal, as this is the first maximum, which indicates the maximum delamination detectability. However, due to man-

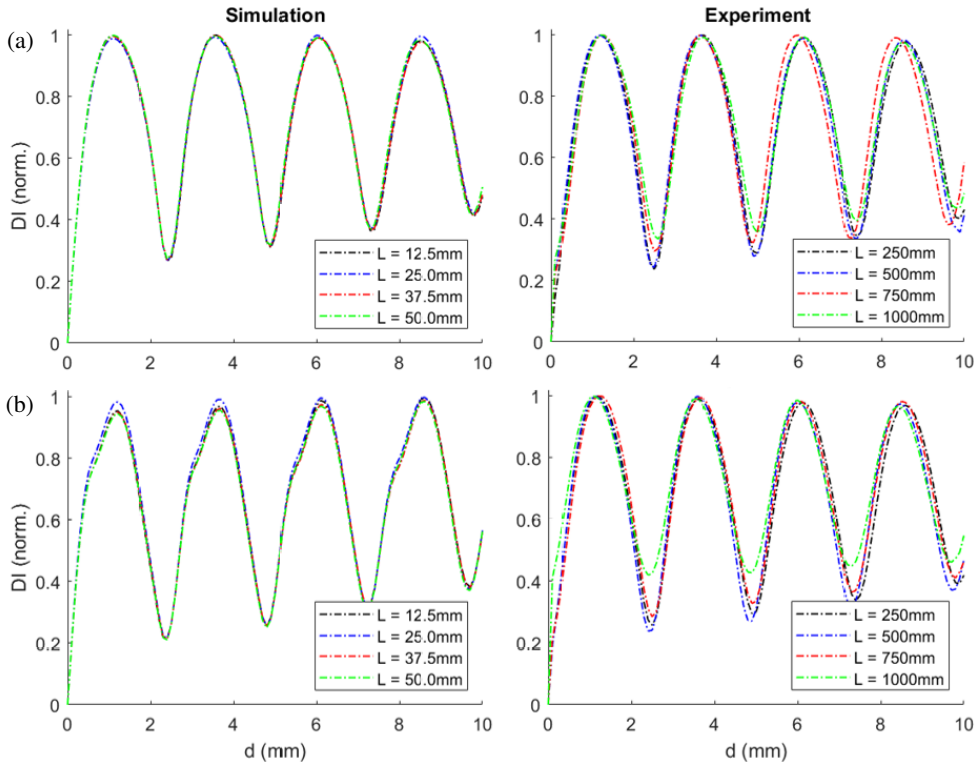

FIGURE 9. DI curves for reference damage #1 directed (a) away from the radar and (b) towards the radar in four different radar distances L. The damage size step is 0.1 mm.

ufacturing tolerances, the effective thickness of the Rohacell sheet was 1.64 mm.

3.2. Radar Signal Data Acquisition

The sR60-12RLi radar from IMST GmbH can operate in both CW and FMCW modes. CW radars emit EM radiation continuously at one frequency. This only enables velocity measurements via the Doppler effect. However, FMCW mode is required to determine the location of targets [4]. The frequency in this work ranges from 57 GHz to 65 GHz. This corresponds to a bandwidth of $B = 8$ GHz. Frequency ramps are linearly increased according to a sawtooth function. With a sampling frequency of the analog digital converter (ADC) $f_{\mathrm{ADC}} = 1$ MHz, the elapsed time per data point $n \in [0, N-1]$ is given by

$$t_n = \frac{n}{f_{\mathrm{ADC}}}. \tag{3}$$

A maximum of $N = 2048$ data points can be recorded by a single ramp. Hence, the total ramp duration is $t_{N-1} = 2.047$ ms.

A chip-integrated patch antenna, which is controlled by a microcontroller unit (MCU), acts as a transmitter and receiver. The reflection signals are mixed with the transmitted signal and detected in the real part without phase shift and in the imaginary part with a phase shift of 90°. The complex signal is transformed into the frequency domain via fast Fourier transform (FFT) directly on the MCU. The frequency axis is based on the definition of the range resolution [24]

$$\delta_R = \frac{c_0}{2B}, \tag{4}$$

which leads to a distance axis of:

$$R_n = \delta_R n. \tag{5}$$

The range resolution depends mainly on the bandwidth B, which is here $\delta_R = 18.74$ mm. It should be noted that δ_R is greater than typical delamination thicknesses. Therefore, it is crucial to consider the signal intensities for the mathematical formulation of a DI in this millimeter wave application.

Due to statistical fluctuations, 20 ramps are recorded for each structural state. One ramp requires a measurement and signal processing time of about 3 s, resulting in a measurement time of 1 min per structural state. The radar is controlled by a standard PC via an SPI cable with a USB connection.

All measurements were carried out under laboratory conditions. Temperature and humidity are assumed to remain constant in order to consider only structural changes in the evaluation of radar signals. In addition, irregular defects, nonuniform air distribution, and the mechanical dynamics of the structure during operation have not been taken into account so far. This means that the results extracted from the measurement data represent a simplification of real-world scenarios.

3.3. Interpretation of Experimental Radar Signals

Figure 7 shows the radar signals for a delamination directed away from the radar in the time and frequency domains at two radar distances $L = 250$ mm and 1000 mm. Five typical delamination thicknesses are compared: $d = 0.1$ mm, 0.2 mm, 0.5 mm, 1 mm, and 2.5 mm. The first two echoes in the frequency domain signals are particularly distinctive. For $L = 0.25$ m, the peaks are detected at 0.26 m and 0.51 m, and

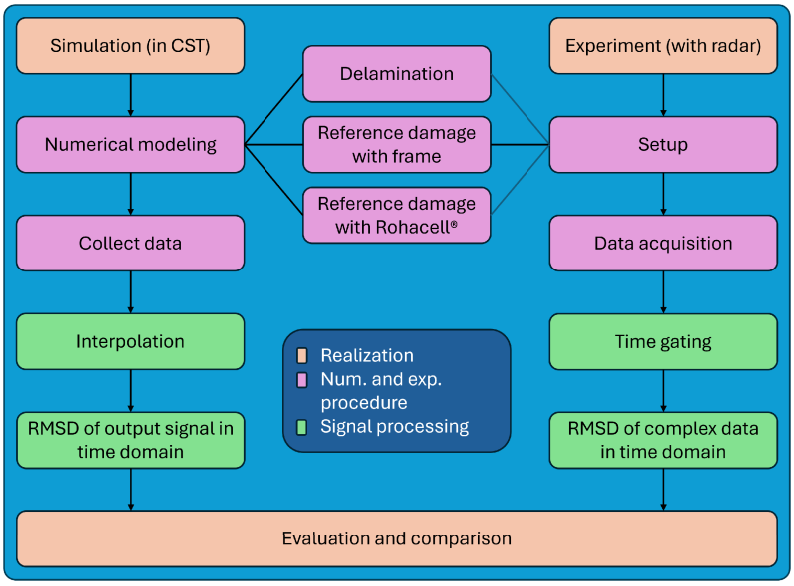

FIGURE 10. Concept of the radar-based SHM system where numerical and experimental are analyzed in three steps to evaluate and detect structural changes at GFRP plates.

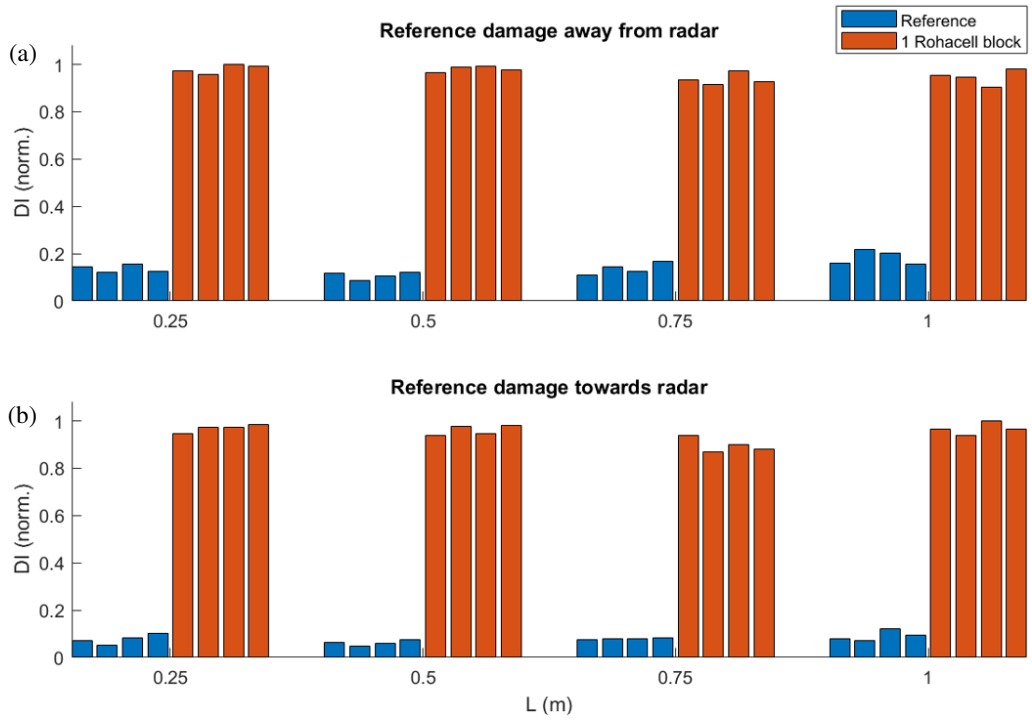

FIGURE 11. Experimental DI for reference damage model #2 (a) directed away from the radar and (b) towards the radar in four different radar distances L. One DI represents the average of five frequency ramps.

for $L = 1$ m, they occur at 1.01 m and 2.00 m. For both radar distances, a peak can also be seen at around 2.23 m due to the reflection of EM waves at the ceiling.

In Figure 7(a), one can see that there is more random noise at the beginning and at the end of the signal. This is caused by the ADC. Hence, a time gate is applied from 0.2 ms to 1.78 ms. The signal intensities between 0.8 ms and 1.3 ms for $d = 1$ mm (green line) are remarkable.

4. NUMERICAL AND EXPERIMENTAL RESULTS

4.1. Signal Processing Using a Damage Indicator Approach

Figure 10 shows that the data processing pipeline for numerical and experimental signals is similar. The evaluation is performed by calculating DIs for simulated and averaged experimental signals in the time domain. Therefore, the root mean square deviation (RMSD) is computed based on the signal dif-

ference between the damaged state S_{dam} and a reference state S_{ref}:

$$\text{DI} = \sqrt{\frac{1}{N}\sum_{n=0}^{N-1} |S_{\text{dam}}[t_n] - S_{\text{ref}}[t_n]|^2}. \quad (6)$$

The equation accounts for the complex-valued nature of the radar signals. The simulation data does not have an imaginary part, so it can be neglected in this equation. Within one graph, the DIs are normalized to 1 for comparability. The DIs are plotted as a function of d in the following subsections. Even though CST uses pulsed signals and the FMCW radar uses continuous intermediate frequency signals, the DIs are the resulting signal responses, which show for both waveforms a periodic trend. The periodicity of the recurring minima and maxima every $\lambda/2$ is discussed by comparing the deviations between simulation and experiment.

4.2. DI Analysis for Delamination

Figure 8 shows the normalized DIs from the simulated and experimental data for a delamination with increasing thickness. A periodic trend can be observed in all cases. The deviations between the minima and maxima of the simulated and experimental DI curves are between 0 mm and 0.3 mm. The DI from the simulated signals shows in particular that the radar distance L has a negligible effect on the overall DI characteristic. The experimental measurements with the wooden plate, in which the delamination is directed towards the radar, show that the DI curves are more similar to each other.

4.3. DI Analysis for Reference Damage #1

Figure 9 depicts the normalized DIs for the simulated and experimental data for reference damage #1. A periodic trend can also be seen here in all cases. The deviations of the minima and maxima of the simulated and experimental DI curves are between 0 mm and 0.2 mm. Compared to Figure 8, the DI curves are smoother, which shows the simplified experimental implementation with the PVC frame. However, the green line for $L = 1000$ mm with the reference damage directed towards the radar shows that the minima are slightly higher than for other radar distances. The periodic trend of the DIs with the wooden plate is slightly different from Figure 8, because the first interface is the erosion protection tape, which has a smaller permittivity than the GFRP plate.

4.4. DI Analysis for Reference Damage #2

Figure 11 shows the normalized DIs from the experimental data for a reference damage #2 with a Rohacell® thickness of 1.64 mm. The DI is based on five averaged frequency ramps leading to four DIs. The analysis includes radar positions 1 and 2. Two aspects should be noted: First, the fluctuations of the DIs for each structural state are small, and second, the difference of the DIs between the structural states relative to each other is significant. In all cases the damage can be clearly identified with the proposed DI approach.

5. CONCLUSIONS

In this work, a reversible damage model for millimeter-wave inspections of GFRP materials was designed, manufactured, and experimentally characterized using numerical and experimental methods. Simulations and measurements were performed in the frequency band from 57 to 65 GHz. The delamination thickness was increased towards and away from the signal source. The DIs showed a periodic trend when the delamination increased. Between simulation and experiment, the maximum deviation of the minima and maxima in the DI curves was 0.3 mm. In the reference damage model with Rohacell® as intermediate layer, there was a clear distinction from the reference state of the intact structure. The radar distance to the structure is approximately negligible compared to the delamination thickness.

In future research, the probability of detection (POD) of the reference damage will be calculated. The reference damage model will also be used to develop algorithms for radar-based SHM systems for various nondestructive applications with composite structures, e.g., in WTBs. Parametric studies will be performed in a climatic chamber to study and compensate for temperature, humidity, and ice formation effects. In the future, it is planned to apply the proposed damage model in field studies on a WT. The binary classification with machine learning methods becomes important, taking into account the large amount of data over all seasonal environmental and operational conditions.

ACKNOWLEDGEMENT

The authors gratefully acknowledge the financial support of this research by the Federal Ministry for Economic Affairs and Climate Action (Grant Number: 03EE2053A).

REFERENCES

[1] Saeed, N. M., "Recent advances in structural health monitoring: Techniques, applications and future directions," *International Journal of Reliability and Safety*, Vol. 18, No. 1, 55–85, 2024.

[2] Hassani, S., M. Mousavi, and A. H. Gandomi, "Structural health monitoring in composite structures: A comprehensive review," *Sensors*, Vol. 22, No. 1, 153, 2021.

[3] Tang, W., J. Blanche, D. Mitchell, S. Harper, and D. Flynn, "Characterisation of composite materials for wind turbines using frequency modulated continuous wave sensing," *Journal of Composites Science*, Vol. 7, No. 2, 75, 2023.

[4] Skolnik, M., *Radar Handbook*, McGraw-Hill, 2008.

[5] Simon, J., T. Kurin, J. Moll, O. Bagemiel, R. Wedel, S. Krause, F. Lurz, A. Nuber, V. Issakov, and V. Krozer, "Embedded radar networks for damage detection in wind turbine blades: Validation in a full-scale fatigue test," *Structural Health Monitoring*, Vol. 22, No. 6, 4252–4263, 2023.

[6] Beziuk, G., T. C. Baum, K. Ghorbani, and K. J. Nicholson, "Structurally integrated radar in an aerospace composite laminate," *IEEE Transactions on Components, Packaging and Manufacturing Technology*, Vol. 11, No. 11, 1835–1843, 2021.

[7] Ciattaglia, G., G. Iadarola, G. Battista, L. Senigagliesi, E. Gambi, P. Castellini, and S. Spinsante, "Displacement evaluation by mmWave FMCW radars: Method and performance metrics," *IEEE Transactions on Instrumentation and Measurement*,

Vol. 73, 1–13, 2024.

[8] Pramudita, A. A., D.-B. Lin, A. A. Dhiyani, H. H. Ryanu, T. Adiprabowo, and E. A. Yudha, "FMCW radar for noncontact bridge structure displacement estimation," *IEEE Transactions on Instrumentation and Measurement*, Vol. 72, 1–14, 2023.

[9] Ma, Z., J. Choi, L. Yang, and H. Sohn, "Structural displacement estimation using accelerometer and FMCW millimeter wave radar," *Mechanical Systems and Signal Processing*, Vol. 182, 109582, 2023.

[10] Keshmiry, A., S. Hassani, M. Mousavi, and U. Dackermann, "Effects of environmental and operational conditions on structural health monitoring and non-destructive testing: A systematic review," *Buildings*, Vol. 13, No. 4, 918, 2023.

[11] Mahendran, J., F. Schenkel, B. Hattenhorst, T. Musch, I. Rolfes, J. Barowski, and C. Schulz, "Temperature and humidity effects on electromagnetic waves utilizing 140 GHz radar measurements," in *2025 IEEE/MTT-S International Microwave Symposium — IMS 2025*, 713–716, San Francisco, CA, USA, 2025.

[12] Simon, J., J. Moll, and V. Krozer, "Trend decomposition for temperature compensation in a radar-based structural health monitoring system of wind turbine blades," *Sensors*, Vol. 24, No. 3, 800, 2024.

[13] Figueiredo, E., G. Park, C. R. Farrar, K. Worden, and J. Figueiras, "Machine learning algorithms for damage detection under operational and environmental variability," *Structural Health Monitoring*, Vol. 10, No. 6, 559–572, 2011.

[14] Streser, E., S. Alipek, M. Rao, J. Simon, J. Moll, P. Kraemer, and V. Krozer, "Radar-based damage detection in a wind turbine blade using convolutional neural networks: A proof-of-concept under fatigue loading," *Sensors*, Vol. 25, No. 11, 3337, 2025.

[15] He, W., W. W.-L. Lai, X. Sui, and A. Giannopoulos, "Delamination characterization in thin asphalt pavement structure using dispersive GPR data," *Construction and Building Materials*, Vol. 402, 132834, 2023.

[16] Liu, J., D. G. Zollinger, and R. L. Lytton, "Detection of delamination in concrete pavements using ground-coupled ground-penetrating radar technique," *Transportation Research Record: Journal of the Transportation Research Board*, Vol. 2087, No. 1, 68–77, 2008.

[17] Popovics, J. S., S. Ham, M. T. Ghasr, and R. Zoughi, "Comparison of synthetic aperture radar and impact-echo imaging for detecting delamination in concrete," in *AIP Conference Proceedings*, Vol. 1581, No. 1, 866–871, Baltimore, MD, USA, 2014.

[18] Tsivouraki, N., K. Tserpes, and I. Sioutis, "Modelling of fatigue delamination growth and prediction of residual tensile strength of thermoplastic coupons," *Materials*, Vol. 17, No. 2, 362, 2024.

[19] Eun, S.-W., W.-H. Choi, H.-K. Jang, J.-H. Shin, J.-B. Kim, and C.-G. Kim, "Effect of delamination on the electromagnetic wave absorbing performance of radar absorbing structures," *Composites Science and Technology*, Vol. 116, 18–25, 2015.

[20] Xu, X., T. Dai, J. Luo, J. Zhao, J. Qiu, S. Chen, and Z. Chen, "Detectability of delamination in laminated CFRPs with diverse stacking sequences using eddy current method with TR pancake coil," *NDT & E International*, Vol. 136, 102814, 2023.

[21] Akbar, M. F., G. N. Jawad, L. R. Danoon, and R. Sloan, "Delamination detection in glass-fibre reinforced polymer (GFRP) using microwave time domain reflectometry," in *2018 15th European Radar Conference (EuRAD)*, 253–256, Madrid, Spain, 2018.

[22] Moll, J., J. Kathol, C.-P. Fritzen, M. Moix-Bonet, M. Rennoch, M. Koerdt, A. S. Herrmann, M. G. R. Sause, and M. Bach, "Open guided waves: Online platform for ultrasonic guided wave measurements," *Structural Health Monitoring*, Vol. 18, No. 5–6, 1903–1914, 2018.

[23] Baron, S., B. Guiffard, and A. Sharaiha, "Polyurethane membranes for flexible centimeter-wave patch antennas," *Journal of Micromechanics and Microengineering*, Vol. 24, No. 7, 075020, 2014.

[24] Jankiraman, M., *FMCW Radar Design*, Artech House, 2018.

[25] Pozar, D. M., *Microwave Engineering*, John Wiley & Sons, 2012.